Author's personal copy

Biomaterials 33 (2012) 9019–9026

Contents lists available at SciVerse ScienceDirect

Biomaterials

journal homepage: www.elsevier.com/locate/biomaterials

Directing tissue morphogenesis via self-assembly of vascular mesenchymal cells

Ting-Hsuan Chen [a], Xiaolu Zhu [a,b,1], Leiting Pan [c,1], Xingjuan Zeng [d], Alan Garfinkel [e,f], Yin Tintut [f], Linda L. Demer [f,g,h], Xin Zhao [d], Chih-Ming Ho [a,h,*]

[a] Mechanical and Aerospace Engineering Department, University of California, Los Angeles, Los Angeles, CA 90095, USA
[b] School of Mechanical Engineering and Jiangsu Key Laboratory for Design and Manufacture of Micro-Nano Biomedical Instruments, Southeast University, JiangNing District, Nanjing 211189, China
[c] Key Laboratory of Weak-Light Nonlinear Photonics, Ministry of Education, TEDA Applied Physics School and School of Physics, Nankai University, Tianjin 300071, China
[d] Institute of Robotics & Automatic Information Systems, Nankai University, Tianjin 300071, China
[e] Department of Integrative Biology and Physiology, University of California, Los Angeles, Los Angeles, CA 90095, USA
[f] Department of Medicine, University of California, Los Angeles, Los Angeles, CA 90095, USA
[g] Department of Physiology, University of California, Los Angeles, Los Angeles, CA 90095, USA
[h] Department of Bioengineering, University of California, Los Angeles, Los Angeles, CA 90095, USA

ARTICLE INFO

Article history:
Received 9 August 2012
Accepted 29 August 2012
Available online 23 September 2012

Keywords:
Micropatterning
Self-assembly
Co-culture
Mesenchymal stem cell

ABSTRACT

Rebuilding injured tissue for regenerative medicine requires technologies to reproduce tissue/biomaterials mimicking the natural morphology. To reconstitute the tissue pattern, current approaches include using scaffolds with specific structure to plate cells, guiding cell spreading, or directly moving cells to desired locations. However, the structural complexity is limited. Also, the artificially-defined patterns are usually disorganized by cellular self-organization in the subsequent tissue development, such as cell migration and cell–cell communication. Here, by working in concert with cellular self-organization rather than against it, we experimentally and mathematically demonstrate a method which directs self-organizing vascular mesenchymal cells (VMCs) to assemble into desired multicellular patterns. Incorporating the inherent chirality of VMCs revealed by interfacing with microengineered substrates and VMCs' spontaneous aggregation, differences in distribution of initial cell plating can be amplified into the formation of striking radial structures or concentric rings, mimicking the cross-sectional structure of liver lobules or osteons, respectively. Furthermore, when co-cultured with VMCs, non-pattern-forming endothelial cells (ECs) tracked along the VMCs and formed a coherent radial or ring pattern in a coordinated manner, indicating that this method is applicable to heterotypical cell organization.

© 2012 Elsevier Ltd. All rights reserved.

1. Introduction

Regenerative medicine aims at cell-based therapy to heal or restore tissue function that has become impaired by chronic degeneration or physical damages [1,2]. The reconstruction of tissue function requires the orchestration of its constituent cells, soluble chemical factors, and extracellular matrix into a spatiotemporal pattern. For example, cardiac function requires the cardiac fibers to assemble into layers with specific orientation angles [3]. Similarly, biochemical and detoxification functions of the hepatic lobule require hepatic cells organizing into a radial network for fluidic transportation of the metabolites [4]. Thus, in addition to providing proper cell types for different applications [5,6], the development of tissue/biomaterial with structural features mimicking the specific spatial pattern is also crucial in tissue regeneration.

To date, considerable efforts have been invested into constructions of scaffolds that allow cell attachment, migration and delivery of biochemical factors [7]. To reconstitute tissue architectural features in microenvironments, diverse attempts have been made to fabricate the scaffold with specific structure to guide cell spreading [8], assemble layers of cultured cell sheets [9,10], directly deposit cells or move cells to chosen locations [11–13]. However, the structural complexity is limited by the mechanical precision of those approaches. Additionally, cellular self-organization, an essential feature in tissue development that uses mechanisms such as cell migration [14] and cell–cell alignment [15], would also defeat and frustrate such artificial attempts, eventually disorganizing the defined morphology.

In natural development, embryogenesis and wound healing heavily rely on self-organized activities. In this manner, tissue-level

* Corresponding author. Mechanical and Aerospace Engineering Department, University of California, Los Angeles, Los Angeles, CA 90095, USA. Tel.: +1 (310) 825 9993; fax: +1 (310) 206 2302.
E-mail address: chihming@seas.ucla.edu (C.-M. Ho).
[1] X.Z. and L.P. contributed equally to this work.

0142-9612/$ – see front matter © 2012 Elsevier Ltd. All rights reserved.
http://dx.doi.org/10.1016/j.biomaterials.2012.08.067

Author's personal copy

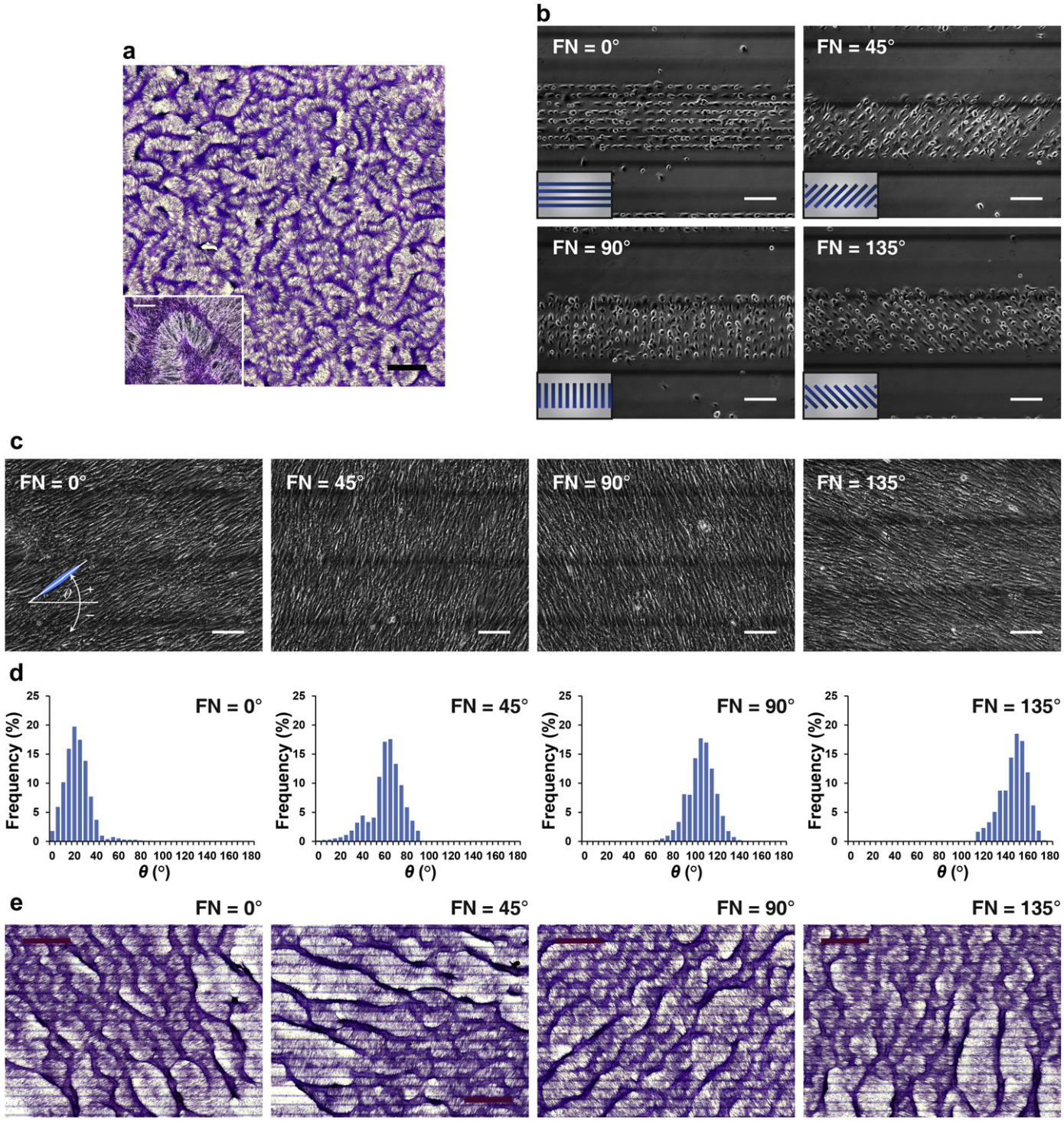

Fig. 1. Coherent cell orientation with respect to the inclination angle of FN/PEG interface. (a) At day 10–14, development of regularly spaced aggregates in a labyrinthine configuration in conventional cell culture. Insets: higher magnification images of multicellular aggregates. Scale bar, 2 mm and 300 μm (inset). (b, c) Phase-contrast microscopy of VMCs plated on parallel 20 μm-wide fibronectin stripes (FN) spaced by 20 μm-wide polyethylene glycol (PEG) stripes within a 300 μm-wide band. The FN stripes oriented at 0°, 45°, 90°, and 135° relative to the horizontal axis. Inset, schematic of a cluster of FN stripes (blue) surrounded by PEG (gray). Images were acquired on (b) day 0 and (c) day 5. Scale bar, 150 μm. (d) Histogram of θ showing convergence to 20 ± 12°, 59 ± 15°, 103 ± 12°, and 145 ± 12° where FN stripes oriented at 0°, 45°, 90°, and 135°, respectively ($N > 10{,}000$ cells; day 5; mean ± S.D.). (e) Development of regularly spaced aggregates aligned at $\theta + 90° = \sim 110°, 150°, 195°$, and 235° when cultured on FN stripes oriented at 0°, 45°, 90°, and 135°, respectively. Scale bar, 1.5 mm. Multicellular ridges were stained purple with hematoxylin in (a) and (e).

structures with intricate patterns are assembled through communication of organizational instructions. Here, by working in concert with cellular self-organization rather than against it, we present an approach for reconstructing tissue/biomaterial via cell-assembly into desired morphologies. Vascular mesenchymal cells (VMCs), which spontaneously migrate and assemble into periodic multicellular aggregates resembling normal tissue (Fig. 1a) [16], were used to reconstitute natural self-organization. Microengineered substrates, which provoke the inherent chirality of VMCs [17], were applied to stimulate the system. Mathematical modeling was

Author's personal copy

employed to design the layout of initial cell distribution. In addition, vascular endothelial cells (ECs) were co-cultured with VMCs to recapitulate the heterogeneity of natural tissue. Integrating the engineered substrates, mathematical modeling, and cellular self-organization, we aim at providing an engineering framework to guide self-organized tissue growth, with implications for building robust and instructive microenvironments for tissue engineering.

2. Materials and methods

2.1. Microengineered substrates

A glass substrate (Precise Glass and Optics, CA) was cleaned, modified with hexamethyldisilazane (HMDS) and coated with photoresist (AZ5214). The photoresist was patterned by ultraviolet exposure, developed (AZ-400K), and treated with oxygen plasma (500 mTorr, 200 W) for 2 min prior to stripping the remaining photoresist by acetone, IPA, and deionized water. For polyethylene glycol (PEG) coating, the HMDS/glass substrates were immersed in 3 mM $C_3H_9O_3Si(C_2H_4O)_{6-9}CH_3$ (Gelest, Inc., PA) dissolved in anhydrous toluene with 1% triethylamine (v/v) (Sigma–Aldrich, St. Louis, MO) for 4 h, followed by ultrasonication in anhydrous toluene, ethanol and deionized water for 5 min, respectively [18]. After drying, the HMDS/PEG substrates were diced into 2 cm × 2 cm chips and stored in desiccators. The titanium reference lines on the reverse side of the chip were fabricated before the preparation of HMDS/PEG substrates.

2.2. Cell culture

Bovine VMCs and ECs were isolated and cultured as described [19,20]. All cells were grown in Dulbecco's Modified Eagle's Medium supplemented with 15% heat inactivated fetal bovine serum and 1% penicillin/streptomycin (10,000 I.U./10,000 μg/ml; all from Mediatech, Inc., VA). Cells were incubated at 37 °C in a humidified incubator (5% CO_2 and 95% air) and passaged every three days.

2.3. Multicellular pattern formation

Each culture was prepared on either 35-mm plastic dishes (200,000 cells per dish) or binary substrates composed of fibronectin (FN) and PEG (200,000 cells per chip) with media changes every three days. For the FN/PEG substrate, the HMDS/PEG substrates were first incubated with FN solution (50 μg ml^{-1}, Sigma–Aldrich, St. Louis, MO) in calcium-/magnesium-free phosphate-buffered saline (Mediatech, Inc., VA) at 4 °C for 15 min, where FN was rapidly adsorbed only to the HMDS regions. After rinsing, VMCs were plated in the FN-coated chip for 30 min (200,000 cells in 500 μl media). After brief washings, only cells adhering to the FN regions remained. At day 10–14, cultures were stained with hematoxylin (Sigma–Aldrich, St. Louis, MO) for 15 min to reveal multicellular aggregates. The panorama images were assembled from a series of images and recombined by panoramic stitching software (PTGui, New House Internet Services BV, Rotterdam, Netherlands). Each image was acquired by an inverted microscope (Eclipse TE 2000, Nikon Instruments Inc., CA).

2.4. VMC/EC co-culture

VMCs and ECs were stained with fluorescent CellTracker™ probes (CellTracker™ Green CMFDA for VMCs and CellTracker™ Red CMTPX for ECs, Life Technologies Corporation, NY) for long-term tracing of these living cells. The dye stock solution was prepared by dissolving lyophilized CellTracker™ probes in high-quality anhydrous dimethylsulfoxide (DMSO) to a final concentration of 10 mM, and then stored at −20 °C, desiccated and protected from light. At the time of staining (day 9 for conventional culture or day 6 for microengineered substrate), both the green and red dye working solutions were prepared by diluting the stock solutions to a final working concentration of 10 μM in serum-free medium. VMCs and ECs grown on 35-mm petri dishes were stained by adding 2 ml of pre-warmed dye solution into each dish and subsequently incubating the cells for 40 min, followed by replacing the dye solution with the fresh pre-warmed serum-free medium and incubating at 37 °C for 30 min. Finally, all the cells were rinsed by phosphate-buffered saline and cultured in growth medium. The next day, the stained ECs (400,000 cells per dish) were trypsinized and added into the VMC culture. Each image was acquired by an inverted microscope (Eclipse TE 2000, Nikon Instruments Inc., CA) on day 15 for conventional culture or day 8–11 for microengineered substrate.

2.5. Time-lapse videomicroscopy

Cultures were incubated in a microscopic thermal stage (HCS60, Instec, Inc., CO) at 37 °C and continuously supplied with premixed 5% CO_2. At day 7, images were acquired at 5 min intervals for a total of 9.5 h using the charge-coupled device and inverted microscope (as above) in bright field. The adequacy of the on-stage incubator was verified by monitoring the proliferation of NIH 3T3 cells in the thermal stage compared with that in a conventional incubator by hemocytometry. Over 100 h of culture, proliferation in the thermal stage remained comparable to that in the conventional incubator [17].

2.6. Image analysis

To determine the orientation angle of local cell alignment, 20 images from phase-contrast microscopy were processed using automated edge-detection software. After adjusting image contrast, the images were made binary, and cells were identified using size and intensity thresholds. Next, for each cell, the long-axis and the orientation angle θ relative to the horizontal axis were determined by an algorithm. Finally, the histogram of θ distribution was determined over all cells.

2.7. Mathematical model

See Supplemental Data for details.

3. Results

3.1. Alignment of VMC aggregates with respect to the inclination angle of substrate interfaces

VMCs, stem cell-like multipotent cells, spontaneously self-organize into a multicellular patterns resembling tissue architectures (Fig. 1a) [16]. This pattern, composed of periodic aggregates in labyrinthine configurations, arises from the local reaction and diffusion of chemical morphogens, as postulated by Turing-type mechanisms [16,21]. Previously we reported that, in addition to the chemical kinetics of morphogens, the inherent symmetry-breaking and motility of the VMCs, as revealed by substrate discontinuities, also plays a role in the developmental process [17]. Incorporating Turing instability, symmetry breaking of VMCs and surface micromachining, we used microengineered substrates consisting of 300 μm-wide bands, which have 20 μm-wide FN stripes (cell adherent substrate) spaced by 20 μm-wide PEG stripes (non-adherent substrate) to elucidate the effect of cellular directionality. The FN stripes within each band were designed to orient at angles of 0°, 45°, 90°, and 135°, with respect to the horizontal axis (Fig. 1b). In addition, each band was spaced by 300 μm-wide PEG band (Fig. 1b; dark lines are titanium on the reverse side used to indicate the boundary of each band). Immediately after plating, VMCs selectively attached to the FN stripes in each band (Fig. 1b). Importantly, these FN stripes did not just spatially confine the cells' initial attachment. When the cells began to propagate across the FN/PEG interface, the differential adhesiveness of substrates triggered an inherent left-right (LR) asymmetry of VMCs, causing preferential right-turning on migration across the interfaces [17]. As the cells spread from FN-coated regions to PEG-coated regions on day 5, this rightward-biased cell migration drove individual spindle-shaped cells to coherently orient at 10–20° relative to the FN/PEG interface, resulting in the cell orientation angle $\theta = 20 \pm 12°$, $59 \pm 15°$, $103 \pm 12°$, and $145 \pm 12°$ (mean ± S.D.) while FN stripes oriented at 0°, 45°, 90°, and 135°, respectively (Fig. 1c, d). At day 10–14, VMCs assembled into periodic and parallel stripes of multicellular aggregates that aligned at approximately $\theta + 90°$, perpendicular to the coherent orientation (Fig. 1e). Thus, the orientation of single-cell and multicellular ridge formation in response to the inclination angle of substrate interfaces suggested an effective stimulus to direct this self-organizing system.

3.2. Theoretical modeling of VMC pattern formation

With the coherent orientation, cells migrated toward discrete aggregates preferentially following the orientation angle (Fig. 2a and Supplemental Video S1). We attribute this anisotropic migration to the increased polarization along their long-axis [22]. Eventually, the specific alignment of the multicellular structures perpendicular to the cell orientation emerged from the anisotropic

Author's personal copy

migration of VMCs along the orientation angle θ. To assist the understanding of the self-organized pattern (labyrinths from conventional culture (Fig. 1a) and parallel stripes from coherent cell orientation (Fig. 1e)), we introduced a mathematical model that simulates the pattern formation based on reaction-diffusion of morphogens and preferential cell migration along the orientation angle [16,17,21,23,24]. As first proposed by Turing [25], pattern formation in biology can often be modeled mathematically by postulating morphogens that react chemically and diffuse. Following the work of Keller, Segel [26] and Maini [23], we modeled our system as the reaction (using Gierer and Meinhardt kinetics) and diffusion of a slowly-diffusing activator, bone morphogenetic protein-2 (BMP-2), u, its rapidly-diffusing inhibitor, matrix gamma-carboxyglutamic acid protein (MGP), v, and cell density, n, reflecting proliferation, cytokinetic motility and chemotactic migration toward activators u, as functions of a 2-dimensional domain (x, y):

$$\frac{\partial u}{\partial t^*} = D\nabla^{*2}u + \gamma\left(\frac{nu^2}{v(1+ku^2)} - cu\right) \quad (1)$$

$$\frac{\partial v}{\partial t^*} = \nabla^{*2}v + \gamma\left(nu^2 - ev\right)$$

$$\frac{\partial n}{\partial t^*} = \sum_{ij} A_{ij}\left[\nabla^{*T} \otimes \left(D_n\nabla^* n - \frac{\chi_0 n}{(k_n+u)^2}\nabla^* u\right)\right]_{ij} + r_n n(1-n)$$

$$A = \begin{bmatrix} b_1\cos^2\theta + b_2\sin^2\theta & (b_1-b_2)\cos\theta\sin\theta \\ (b_1-b_2)\cos\theta\sin\theta & b_1\sin^2\theta + b_2\cos^2\theta \end{bmatrix}$$

Supplementary video related to this article can be found at http://dx.doi.org/10.1016/j.biomaterials.2012.08.067.

(See Supplemental Data for detailed mathematical model and parameter estimation [16,23,24,27–29]). Importantly, under the influence of the diffusion and reaction of BMP-2 and MGP, the preferred cell migration along the coherent orientation was modeled by b_1 and b_2, adjustable parameters representing the differential migration speed along the principal axes described as vectors $(\cos\theta, \sin\theta)$ and $(-\sin\theta, \cos\theta)$, where $\theta(x, y)$ is the orientation angle as a function of space (Fig. 2b). For the isotropic migration ($b_1 = 1$, $b_2 = 1$) representing the conventional culture, the simulation produced labyrinthine patterns of $n(x, y)$ (darker areas representing higher cell density) over the computational domain (Fig. 2c), consistent with the observation in conventional culture (Fig. 1a). With the preferential cell migration at different orientation angles ($b_1 = 1$, $b_2 = 10^{-6}$, $\theta = 20°$, $60°$, $105°$, or $145°$ throughout the domain), the simulation produced stripes aligned at $\theta + 90°$ (Fig. 2d), consistent with the multicellular ridges in our experiments (Fig. 1e). Thus, the reaction-diffusion model, together with anisotropic migration guided by coherent orientation, provides a theoretical foundation for the development of multicellular organization into tissue.

3.3. Radial structure or concentric rings formed by homotypic or heterotypic cell organization

We used the mathematical model to assist the design of an engineering strategy for desired multicellular structures. Patterns with radial symmetry and concentric rings, such as the basic structure of liver lobules or transverse sections of osteons in compact bones, are commonly seen in tissue architecture. As shown above, the orientation angle θ plays a critical role in guiding this self-organizing system, and can be controlled by

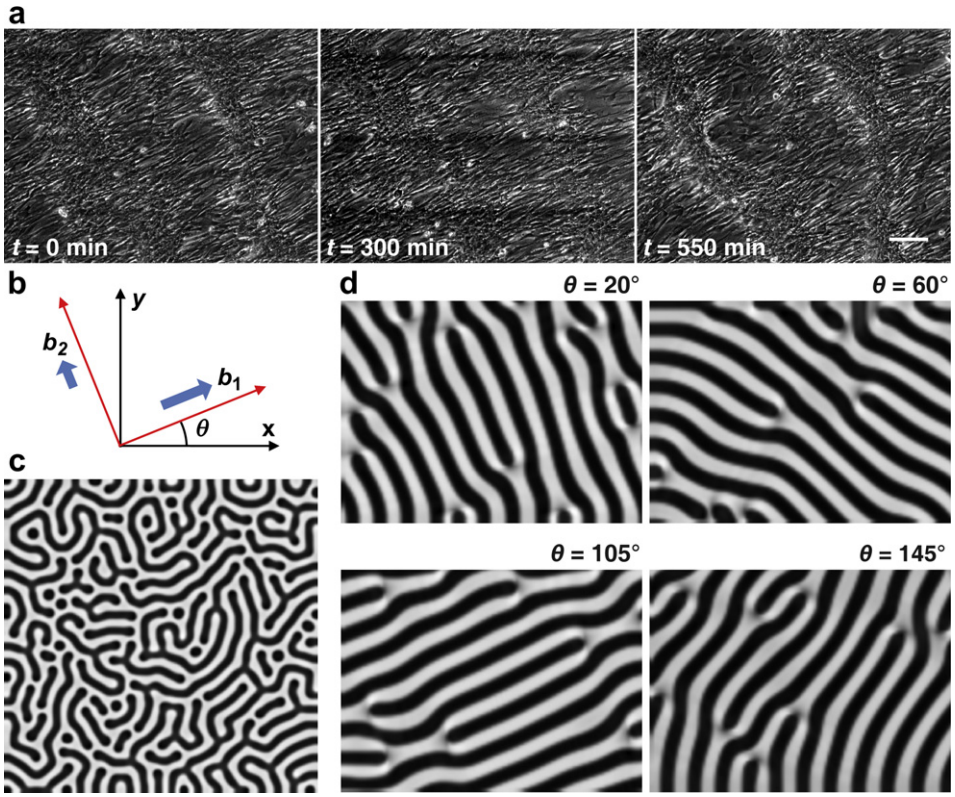

Fig. 2. Theoretical modeling of VMC pattern formation. (a) Time-lapse videomicroscopy of anisotropic cell migration following the coherent orientation. Scale bar, 150 μm. (b) Schematic of coefficients, b_1 and b_2, for principal directions of preferential cell migration. (c) Simulation results of $n(x, y)$ with darker areas representing higher cell density yielding labyrinthine patterns ($b_1 = 1$, $b_2 = 1$). (d) Simulation results of $n(x, y)$ with darker areas representing higher cell density yielding stripe patterns with angular alignment ($b_1 = 1$, $b_2 = 10^{-6}$, $\theta = 20°$, $60°$, $105°$, or $145°$). Model parameters: $D = 0.005$, $\gamma = 65000$, $k = 0.28$, $c = 0.01$, $e = 0.02$, $D_n = 0.06$, $\chi_0 = 0.04$, $k_n = 1$, $r = 322$, $t^* = 1$ (total time).

Author's personal copy

micropatterning. To engineer the cell patterns to resemble the tissue morphology, we combined the micropatterning and the mathematical model to determine the spatial distribution of orientation angle $\theta(x, y)$. In a circle equally divided into 12 partitions, we started from simulating the cell orientation θ in each partition to align either to peripheral or to centripetal directions (Fig. 3a). Numerical simulations using peripheral orientation yielded radial patterns $n(x, y)$ resembling the vascular structure in liver lobules (Fig. 3b). In contrast, with centripetal orientation, the model led to concentric rings of $n(x, y)$, resembling the cross-sectional structure of osteons (Fig. 3b). Furthermore, since natural tissues often consist of multiple, repeated functional units such as osteons and liver lobules in a hierarchical system, we reconstituted it using smaller circles with 6 equally divided partitions arranged according to hexagonal packing. Again, peripheral or centripetal directions in each small circle yielded units of radial patterns or concentric rings, and those units could be hexagonally packed to resemble the natural hierarchical structure (Fig. 3c).

To experimentally validate the mathematical predictions, the orientations of the FN stripes were adjusted according to the desired orientation $\theta^*(x, y)$. Importantly, to implement a desired θ^*, the FN stripes within each band were rotated to $(\theta^* - 20^\circ)$ to compensate for the VMCs' LR asymmetry, which leads to 20° cell orientation relative to the FN/PEG interface (Fig. 1c, d). For example, to implement θ^* as 90°, the FN stripes were rotated by 70° (Fig. 3d and Supplemental Fig. 1). In addition, each 300 μm-wide band was spaced in parallel with the 300 μm-wide PEG band to unify the θ^* distribution within each partition (See Fig. 3d and Supplemental Fig. 1 for an example of the peripheral orientation in 6 equal partitions). Consistent with the mathematical modeling, VMCs formed radial or concentric ring patterns when θ^* was aligned in a peripheral or centripetal manner, respectively (Fig. 3e), and they could also be arranged in a hexagonal packing (Fig. 3f). Taking together, through the combination of mathematical modeling and microengineering, we demonstrated that substrate interfaces can predictably control

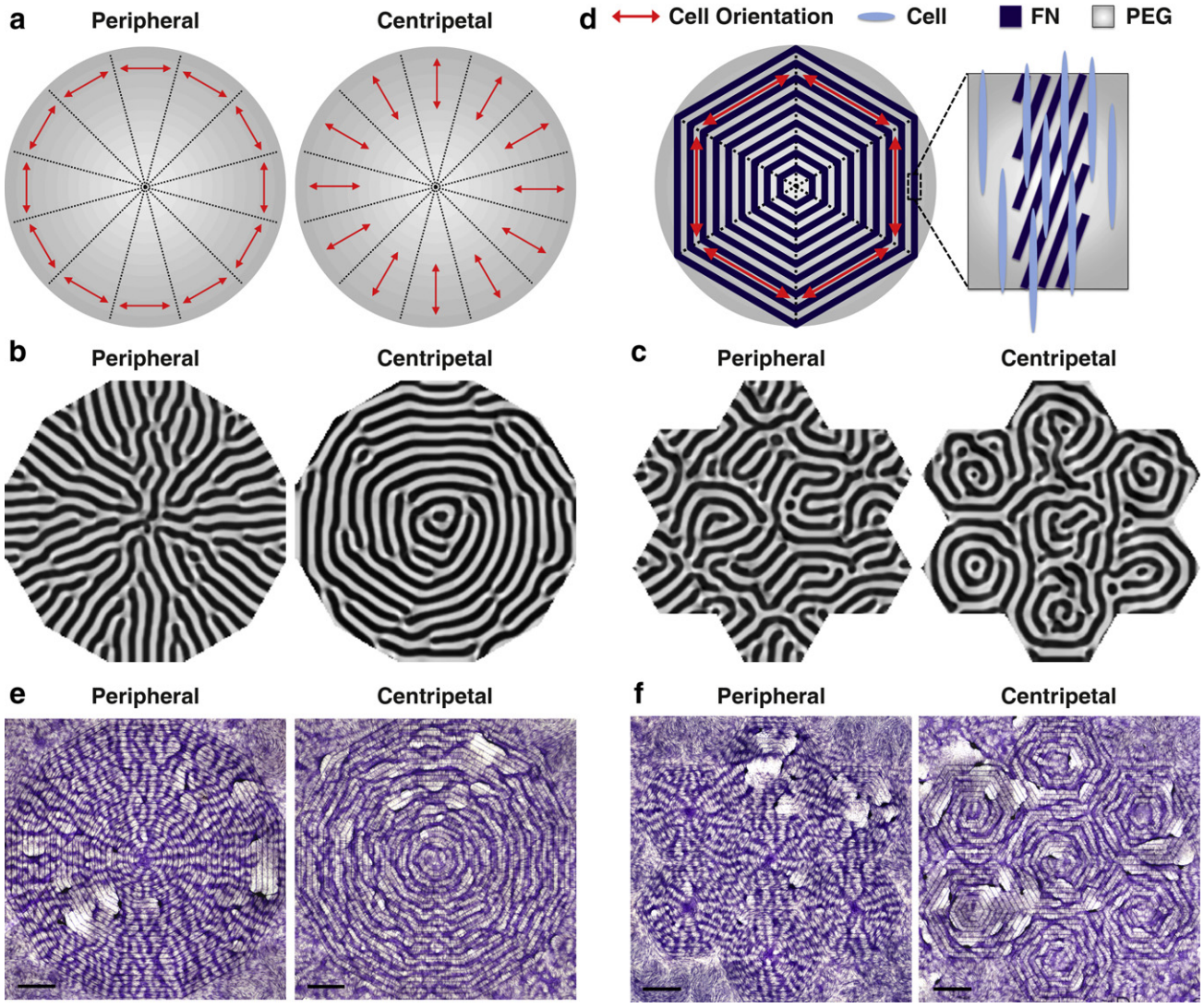

Fig. 3. Directed pattern formation using model predictions and controlled cell orientation. (a) Schematics of θ distribution. (b) Computational simulations showing $n(x, y)$ as a single pattern of radial structures or concentric rings. (c) Computational simulations showing $n(x, y)$ as 6 repeated radial or ring patterns in a hexagonal packing. (d) Schematics of desired θ^* as peripheral orientation in 6 equal partitions. The FN stripes within each 300 μm-wide band were rotated to $\theta^* - 20^\circ$ to compensate for the VMCs' left-right asymmetry which leads to 20° cell orientation relative to the FN/PEG interface. In this example, to implement the desired θ^* as 30°, 90°, and 150° relative to the horizontal axis, the FN stripes in each band were designed as 10°, 70°, and 130°, respectively. Furthermore, each 300 μm-wide band was spaced in parallel with the 300 μm-wide PEG band to unify the θ^* distribution within each partition. (e) VMC patterns formed as radial structures or concentric rings. Scale bar, 2 mm (f) VMC patterns formed as 6 repeated radial or ring patterns in a hexagonal packing. Scale bar, 2 mm. Multicellular ridges were stained purple with hematoxylin in (e) and (f).

Author's personal copy

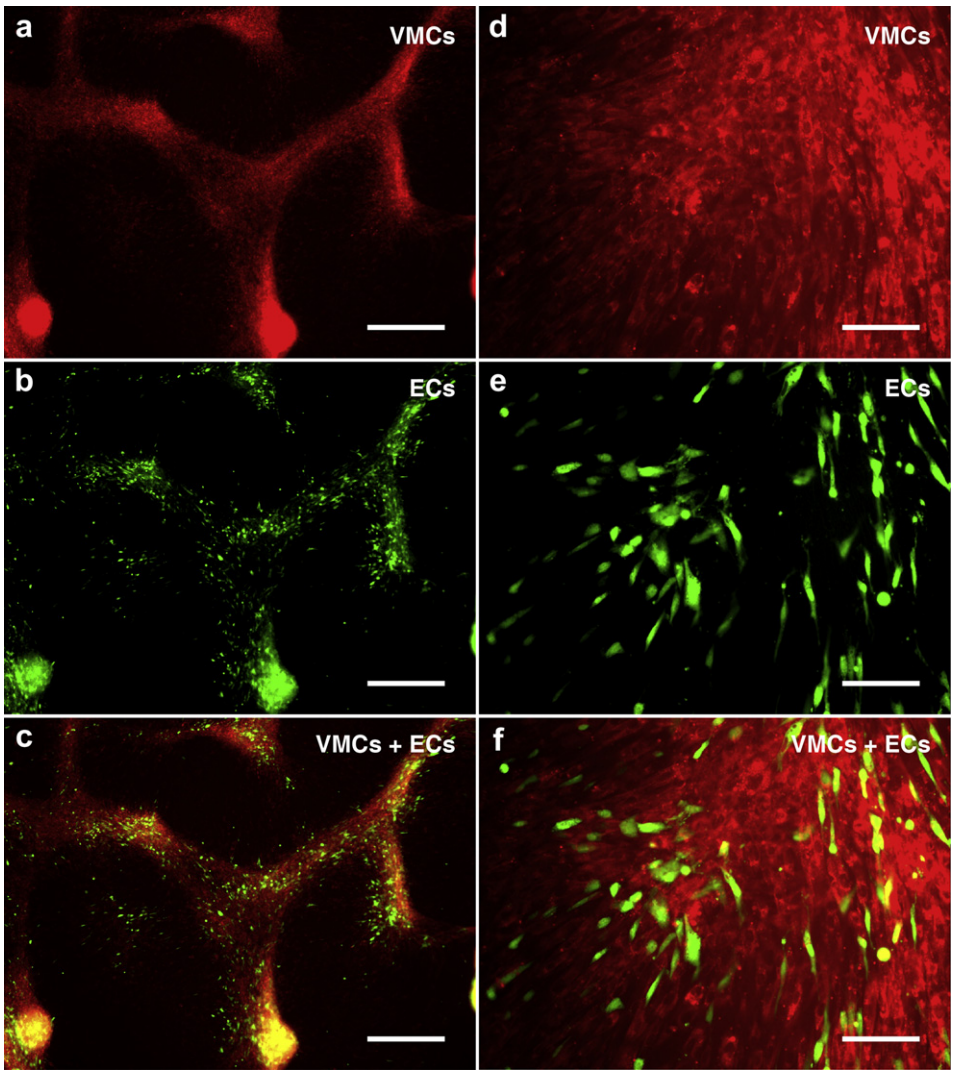

Fig. 4. VMC and EC co-culture stained with fluorescent CellTracker™ probes, where VMCs were stained by Red CMTPX and ECs were stained by Green CMFDA on day 9 prior to plating ECs into VMC culture on day 10. (a–c) At day 15, ECs and VMCs forming (c) heterotypical organizations assembled by both (a) VMCs and (b) ECs. Scale bar, 500 μm (d–f) Higher magnification images of (f) heterotypical aggregates showing the coherent alignment between (d) VMCs and (e) ECs. Scale bar, 100 μm. (For interpretation of the references to color in this figure legend, the reader is referred to the web version of this article.)

cellular self-organization in a manner recapitulating natural tissue development and morphology.

In addition to the morphology formed by homotypic cell types, natural tissue consists of heterotypic cell types, e.g., layers of endothelial cells and smooth muscle cells in the artery wall. To recapitulate the heterogeneity in natural tissue, vascular endothelial cells (ECs) were co-cultured with VMCs. In the absence of VMCs, ECs formed the confluent endothelial cobblestone pattern seen in conventional EC culture (Supplemental Fig. 2). However, in the presence of VMCs underneath ECs, the ECs tracked along aggregating VMCs, forming coordinated multicellular structures composed of both cell types, as ECs aligned with the VMCs' morphology (Fig. 4). As such, using the same control scheme which modulates VMC pattern formation on microengineered substrates, we engineered the formation of composite architectures by VMCs and ECs that coherently aligned into patterns of radial structures and concentric rings (Fig. 5). Thus, the present method is applicable to heterotypical cell organization even when one of the cell types does not by itself possess pattern forming capability.

4. Discussion

Tissue morphogenesis is governed by a combination of self-organizational behavior, including cell alignment, migration, and aggregation. For example, sheets of cells collectively migrate, resulting in three germ layers during gastrulation in embryogenesis [30]. Multicellular aggregates also generate spatial patterns of cell proliferation via the emergence of mechanical stress, which is also essential for folding, expanding, or deforming tissues into specific forms [31]. Despite the fact that self-organization is well-acknowledged in developmental biology, it creates both challenges and opportunities in the context of tissue engineering. Here, our framework demonstrates the feasibility of using self-organization. The incorporation of intrinsic cell chirality, cell migration, and cell–cell aggregation, shows a completely different route for designing and reconstructing biomaterial/tissue with minimum engineering efforts. Inspired by natural development, we envision this direction would leverage the knowledge to engineer the appropriate materials and microenvironments necessary for tissue formation or organ-specific architectures.

Author's personal copy

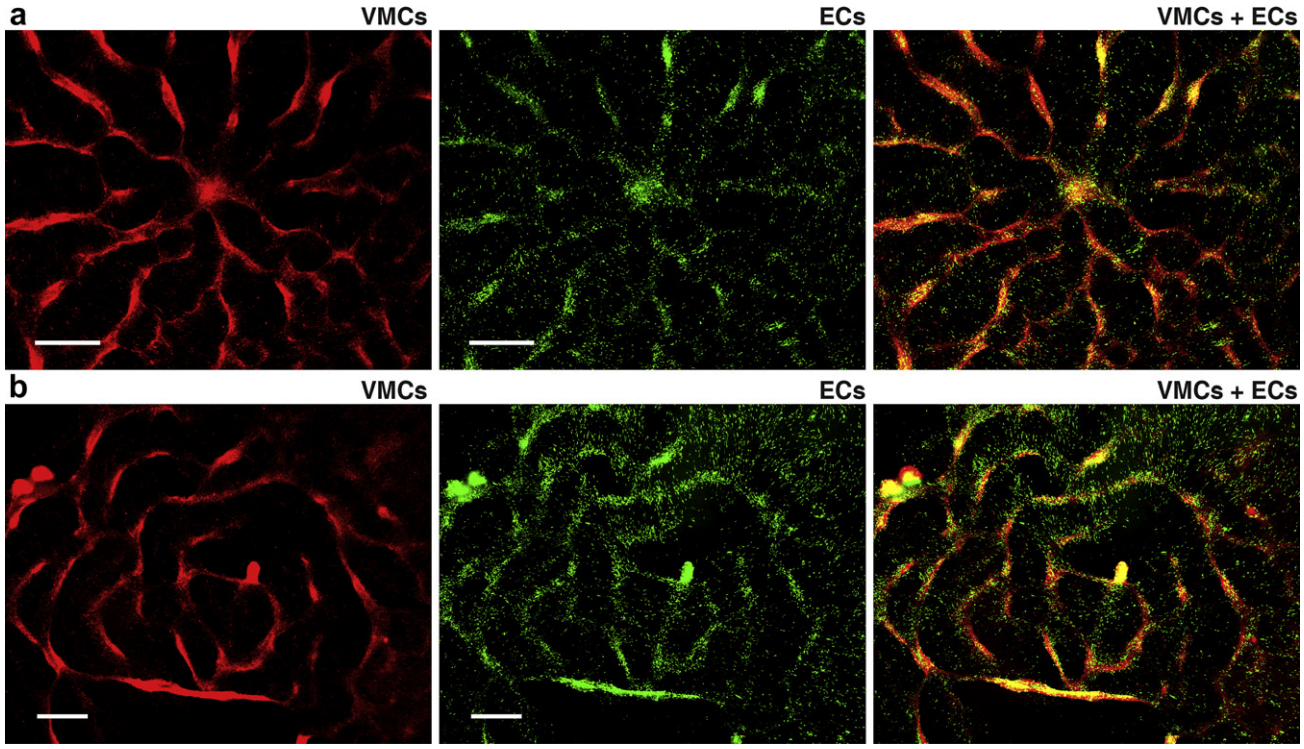

Fig. 5. Coherent alignment of VMCs and ECs via heterotypical coordination. (a) Radial structure composed of VMCs (red) and ECs (green). Scale bar, 1 mm. (b) Concentric rings composed of VMCs (red) and ECs (green). Scale bar, 1 mm.

The 10–20° orientation angle relative to the FN/PEG interface results of the inherent chirality of VMCs mediated by stress fiber accumulation, as reported previously [17]. Interestingly, one day after plating, cells in contact with the FN remained aligned with the FN stripes, but aligned randomly after migrating onto the pure PEG regions (Supplemental Fig. 3). Given that the 10–20° cell orientation appears after confluence (Fig. 1c), the course of cell spreading suggests that the cell reorientation involves the migration from FN stripes to PEG regions rather than a "rotation" on the FN stripes. It is consistent with the findings that the propagation of cell alignment requires rotational inertia, i.e. the resistance of cells to rotate [15]. Although it is unlikely that the rotational inertia of VMCs was due to the fusing into skeletal muscle as reported previously [15], the spindle-shape of VMCs may already preserve the rotational resistance necessary for the alignment propagation.

The anisotropic cell migration due to the increased polarization along the cell's long-axis is also consistent with the results that cells confined in narrow channels (10 μm) migrate faster than cells in wide channels (>40 μm) or on unconstrained 2D surfaces [22]. As suggested, the stress fibers strongly co-aligned with the long axis of the cell, which enhanced actomyosin traction and thus restricted the polarization along the cell long axis. In our VMC culture, the coherent cell–cell alignment at confluence also creates a physical confinement similar to the narrowed channel, e.g., the stress fibers strongly co-aligned with the long axis of the cells. Thus, the coherent orientation may reinforce the anisotropic migration via the alignment of actomyosin traction, providing an essential component to direct tissue morphogenesis.

5. Conclusion

Producing tissue-like materials with desired spatial patterns plays a crucial role in tissue regeneration. Here, combining theoretical modeling and microengineered cell culture, we demonstrate an engineering strategy that integrates the asymmetry of VMCs triggered by substrate discontinuities, multicellular organization via reaction-diffusion kinetics, and the applicability of heterotypical cell coordination. Importantly, as opposed to allocating cells to desired locations, the use of morphogenetic activity, e.g. cell migration and aggregation observed in embryogenesis and wound healing, permits the recapitulation of normal tissue architecture in a more natural way. This approach shows the potential to assist cell-based therapies to restore, rebuild, or improve a functional replacement for regenerative tissue engineering.

Acknowledgments

This research was supported by grants from the National Science Foundation (gs1) (SINAM 00006047 and BECS EFRI-1025073) and the National Institutes of Health (gs2) (HL081202 and DK081346). X. Zhu is supported by the Joint Ph.D. Training Program of China Scholarship Council (gs3) (No. 2011609045), Scientific Research Foundation of Graduate School of Southeast University (gs4) (No. YBJJ1020) and Ph.D. Graduate Academic Award from Ministry of Education of China (gs5) (2010-SEU). X. Zeng and X. Zhao were supported by grants from National Natural Science Foundation of China (gs6) (No. 91023045 and No. 61273341) and National High Technology Research and Development Program of China (gs7) (863 program, No. 2009AA043703 and No. 2012AA040406). L. Pan is supported by 111 Project (gs8) (No. B07013), the Specialized Research Fund for the Doctoral Program of Higher Education (gs9) (No. 20110031120004).

Appendix A. Supplementary data

Supplementary data related to this article can be found at http://dx.doi.org/10.1016/j.biomaterials.2012.08.067.

Author's personal copy

References

[1] Berthiaume F, Maguire TJ, Yarmush ML. Tissue engineering and regenerative medicine: history, progress, and challenges. Annu Rev Chem Biomol Eng 2011;2:403–30.

[2] Vacanti JP, Langer R. Tissue engineering: the design and fabrication of living replacement devices for surgical reconstruction and transplantation. Lancet 1999;354(9176):SI32–4.

[3] Streeter Jr DD, Spotnitz HM, Patel DP, Ross Jr J, Sonnenblick EH. Fiber orientation in the canine left ventricle during diastole and systole. Circ Res 1969; 24(3):339–47.

[4] McCuskey RS. Morphological mechanisms for regulating blood flow through hepatic sinusoids. Liver 2000;20(1):3–7.

[5] Tsutsui H, Valamehr B, Hindoyan A, Qiao R, Ding X, Guo S, et al. An optimized small molecule inhibitor cocktail supports long-term maintenance of human embryonic stem cells. Nat Commun 2011;2:167.

[6] Mimeault M, Hauke R, Batra SK. Stem cells: a revolution in therapeutics – recent advances in stem cell biology and their therapeutic applications in regenerative medicine and cancer therapies. Clin Pharmacol Ther 2007;82(3): 252–64.

[7] Hutmacher DW. Scaffold design and fabrication technologies for engineering tissues – state of the art and future perspectives. J Biomater Sci Polym Ed 2001;12(1):107–24.

[8] Tsang VL, Bhatia SN. Three-dimensional tissue fabrication. Adv Drug Deliv Rev 2004;56(11):1635–47.

[9] Shimizu T, Yamato M, Kikuchi A, Okano T. Cell sheet engineering for myocardial tissue reconstruction. Biomaterials 2003;24(13):2309–16.

[10] Yang J, Yamato M, Shimizu T, Sekine H, Ohashi K, Kanzaki M, et al. Reconstruction of functional tissues with cell sheet engineering. Biomaterials 2007; 28(34):5033–43.

[11] Mironov V, Boland T, Trusk T, Forgacs G, Markwald RR. Organ printing: computer-aided jet-based 3D tissue engineering. Trends Biotechnol 2003; 21(4):157–61.

[12] Odde DJ, Renn MJ. Laser-guided direct writing of living cells. Biotechnol Bioeng 2000;67(3):312–8.

[13] Ho C-T, Lin R-Z, Chang W-Y, Chang H-Y, Liu C-H. Rapid heterogeneous liver-cell on-chip patterning via the enhanced field-induced dielectrophoresis trap. Lab Chip 2006;6(6):724–34.

[14] Li S, Bhatia S, Hu YL, Shin YT, Li YS, Usami S, et al. Effects of morphological patterning on endothelial cell migration. Biorheology 2001;38(2–3):101–8.

[15] Junkin M, Leung SL, Whitman S, Gregorio CC, Wong PK. Cellular self-organization by autocatalytic alignment feedback. J Cell Sci 2011;124(24): 4213–20.

[16] Garfinkel A, Tintut Y, Petrasek D, Boström K, Demer LL. Pattern formation by vascular mesenchymal cells. Proc Natl Acad Sci USA 2004;101(25):9247–50.

[17] Chen T-H, Hsu JJ, Zhao X, Guo C, Wong MN, Huang Y, et al. Left-right symmetry breaking in tissue morphogenesis via cytoskeletal mechanics. Circ Res 2012;110(4):551–9.

[18] Li N, Ho C-M. Photolithographic patterning of organosilane monolayer for generating large area two-dimensional B lymphocyte arrays. Lab Chip 2008; 8(12):2105–12.

[19] Hsiai TK, Cho SK, Reddy S, Hama S, Navab M, Demer LL, et al. Pulsatile flow regulates monocyte adhesion to oxidized lipid-induced endothelial cells. Arterioscler Thromb Vasc Biol 2001;21(11):1770–6.

[20] Boström K, Watson KE, Horn S, Wortham C, Herman IM, Demer LL. Bone morphogenetic protein expression in human atherosclerotic lesions. J Clin Invest 1993;91(4):1800–9.

[21] Chen T-H, Guo C, Zhao X, Yao Y, Boström KI, Wong MN, et al. Patterns of periodic holes created by increased cell motility. Interface Focus 2012;2(4): 457–64.

[22] Pathak A, Kumar S. Independent regulation of tumor cell migration by matrix stiffness and confinement. Proc Natl Acad Sci USA 2012;109(26):10334–9.

[23] Maini PK, Sean McElwain DL, Leavesley DI. Traveling wave model to interpret a wound-healing cell migration assay for human peritoneal mesothelial cells. Tissue Eng 2004;10(3/4):475–82.

[24] Painter KJ, Maini PK, Othmer HG. Stripe formation in juvenile Pomacanthus explained by a generalized Turing mechanism with chemotaxis. Proc Natl Acad Sci USA 1999;96(10):5549–54.

[25] Turing AM. The chemical basis of morphogenesis. Phil Trans R Soc Lond B 1952;237(641):37–72.

[26] Keller EF, Segel LA. Traveling bands of chemotactic bacteria: a theoretical analysis. J Theor Biol 1971;30(2):235–48.

[27] DiMilla PA, Quinn JA, Albelda SM, Lauffenburger DA. Measurement of individual cell migration parameters for human tissue cells. AIChE J 1992;38(7):1092–104.

[28] Kim N-G, Koh E, Chen X, Gumbiner BM. E-cadherin mediates contact inhibition of proliferation through Hippo signaling-pathway components. Proc Natl Acad Sci USA 2011;108(29):11930–5.

[29] Willette RN, Gu JL, Lysko PG, Anderson KM, Minehart H, Yue T-L. BMP-2 gene expression and effects on human vascular smooth muscle cells. J Vasc Res 1999;36(2):120–5.

[30] Ridley AJ, Schwartz MA, Burridge K, Firtel RA, Ginsberg MH, Borisy G, et al. Cell migration: integrating signals from front to back. Science 2003;302(5651): 1704–9.

[31] Nelson CM, Jean RP, Tan JL, Liu WF, Sniadecki NJ, Spector AA, et al. Emergent patterns of growth controlled by multicellular form and mechanics. Proc Natl Acad Sci USA 2005;102(33):11594–9.